

Magnetic field measurement system based on rotating PCB coils

Gianluca Nicosia¹, Joe DiMarco²

¹*Politecnico di Milano*, ²*Fermilab Technical Division*

September 26, 2014

Contents

1	Introduction	2
1.1	Rotating coil in magnetic field	2
1.2	Two dimensional multipole field	2
1.3	Bucking	3
2	Set-up and noise analysis	4
2.1	DAQ	4
2.1.1	NI-4462	4
2.2	Probes	5
2.2.1	PCB probe	5
2.2.2	Morgan probe	6
2.3	Stepper motor	6
2.4	Power supply	7
2.5	Conclusion	7
3	LABView VI	8
4	Measures	9
4.1	Dipole magnet	9
4.2	Quadrupole magnet	11
5	Conclusions	11
A	Additional tables	13

Abstract

This report presents the work carried out under the supervision of Joe DiMarco by Gianluca Nicosia as Summer Intern at Fermilab Technical Division, Magnet Systems section. The internship was focused on developing a magnetic field measurement system in LabVIEW and MATLAB implementing preexisting scripts and using it to analyze the performances of rotating PCB coils comparing them to more traditional machine-wound harmonic coils. After a brief introduction about the physics of multipole magnetic fields and their measurements, a description of the acquisition system is presented, discussing its limitations. Then the PCB probe and the Morgan probe are characterized in terms of noise. Finally, a set of measures performed using both PCB and Morgan probes on a quadrupole and on a dipole magnet is discussed in order to show the peculiarities of each sensor.

1 Introduction

1.1 Rotating coil in magnetic field

Induction coils, also known as *search coils*, are a kind of sensors employed in magnetic field measurements. They are based on the well known Faraday's Induction Law:

$$\mathcal{E} = -\frac{d\Phi}{dt} = -\frac{d}{dt} \iint_A \mathbf{B} \cdot \mathbf{nd}A = -\iint_A \frac{d\mathbf{B}}{dt} \cdot \mathbf{nd}A - \iint_{\partial A} \mathbf{v} \times \mathbf{B} dl \quad (1)$$

a net variation of magnetic flux Φ through a single winding of area A generates an electromotive force \mathcal{E} . It can be induced in two ways: by a time-varying magnetic field or by a displacement or deformation of the coil with local velocity \mathbf{v} . *Fixed-coils* are employed if the magnetic field is not constant, while *rotating coils* (also known as *harmonic coils*) are used to characterize a constant magnetic field [1]. The flux is obtained integrating the output voltage.

$$\Phi - \Phi_0 = -\int_0^t \mathcal{E} dt$$

This expression is interesting from the signal analysis standpoint. As a matter of fact, integration implies that the coil output is intrinsically low-pass filtered to obtain the quantity of interest, thus strongly limiting white noise bandwidth. However, any voltage offset due to the acquisition system will cause a drift that could negatively affect the measure. This problem can be limited by introducing a digital DC component suppression subtracting from the acquired voltage the average value of all the acquired samples.

Another important aspect to keep in mind when dealing with search coils is their circuit model. As these sensors are usually used at low frequency (under 10 kHz), they can be represented just as a voltage source and a resistance, disregarding parasitic capacitances and inductors [1]. In figure 1, R_{coil} represents the coil output resistance, while R_{in} is the input impedance of the acquisition system. If R_{coil} is not negligible with respect to R_{in} , there will be an important signal loss due to voltage partition.

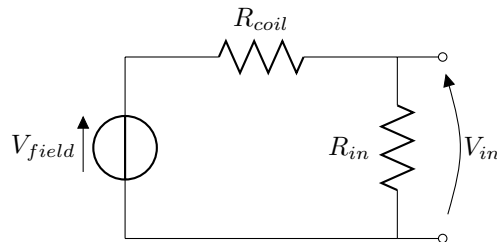


Figure 1: Low-frequency lumped parameter model

1.2 Two dimensional multipole field

Let's consider a region of space free of charges and current. Let's also exclude the presence of propagating electromagnetic waves. From Maxwell's fields equations, any magnetic field in this region must satisfy

$$\nabla \cdot \mathbf{B} = 0 \quad (2)$$

$$\nabla \times \mathbf{B} = 0 \quad (3)$$

It can be shown [5] that a magnetic field $\mathbf{B} = (B_x, B_y, B_z)$ with B_z constant, like in the case of a magnetic field inside a particle accelerator, and the other two components given by

$$B_y + iB_x = \overline{C_n}(x + iy)^{n-1} = \overline{C_n}z^{n-1} \quad \overline{C_n} \in \mathbb{C}, n \in \mathbb{N} \quad (4)$$

satisfies equations 2 and 3. Equation 4 represents a *multipole field*: n is the order of the multipole, while \overline{C}_n is a complex constant. For example, $n = 1$ is a dipole field, $n = 2$ is a quadrupole field. Thus, a generic magnetic field can be written as the superposition of an infinite number of pure multipole fields.

$$B_y + iB_x = \sum_{n=1}^{\infty} \overline{C}_n z^{n-1} \quad (5)$$

This is simply a 2D power series expansion with complex coefficients $\overline{C}_n = \overline{B}_n + i\overline{A}_n$: the harmonics. They represent the strength of the n -th multipole. \overline{B}_n and \overline{A}_n represent, respectively, the normal and skew components of the n -th multipole. As the units of \overline{C}_n depends on the order of the multipole ($[\overline{C}_1] = \text{T}$, $[\overline{C}_2] = \text{T m}^{-1}$), it is convenient to normalize with respect to a reference radius R_r .

$$B_y + iB_x = \sum_{n=1}^{\infty} C_n \left(\frac{z}{R_r} \right)^{n-1} \quad (6)$$

The results presented in section 4 present an additional normalization: the n -th harmonic has been divided by the main field component B_M and multiplied by a factor of 10^4 . This is a standard representational of the error field components.

$$c_n = b_n + ia_n = 10^4 \frac{C_n}{B_M} \quad (7)$$

Harmonics can be easily measured starting from the flux. As a matter of fact, it can be shown [3] [4] that the angular magnetic flux through a rotating coil can be expressed in a Fourier Series-like way:

$$\Phi(\theta) = \text{Re} \left(\sum_{n=1} C_n K_n e^{in\theta} \right) \quad (8)$$

K_n is the winding sensitivity and is defined as [3]

$$K_n = \sum_{j=1}^{N_{wires}} \frac{L_j R_r}{n} \left(\frac{x_j + iy_j}{R_r} \right)^n (-1)^j \quad (9)$$

where

- L_j is the length of the j -th wire
- $(-1)^j$ accounts for the current direction in each wire
- x_j, y_j are the locations of the j -th wire with respect to the rotation axis

Thus, to determine the harmonics it is sufficient to compute the FFT of the flux, compute the complex Fourier coefficients F_n and divide them by the complex sensitivity.

$$C_n = \frac{F_n}{K_n} \quad (10)$$

1.3 Bucking

To accurately measure higher order harmonics it is necessary to connect the coils in such a fashion as to suppress the signal of the main field component [1]. This will consequently suppress spurious harmonics due to coil vibrations. This technique is called *bucking*.

Figure 2 shows, as an example, a dipole bucking scheme. It is made up of two identical coils: the first on top provides the so-called absolute field, the one on the bottom is connected in series opposition to the former and rotates at smaller radius and different chirality [2]. In this way, the output ideally contains only the error field. The results shown in section 4 employ dipole, quadrupole and sextupole bucked signals. This approach is used in the rotating PCB probe under analysis, while Morgan probes use an opposite approach: instead of suppressing one multipole, the geometry of each coil provides just one pure multipole (and its allowed harmonics), and suppresses all others. Details on how this kind of technique works are beyond the scope of this report.

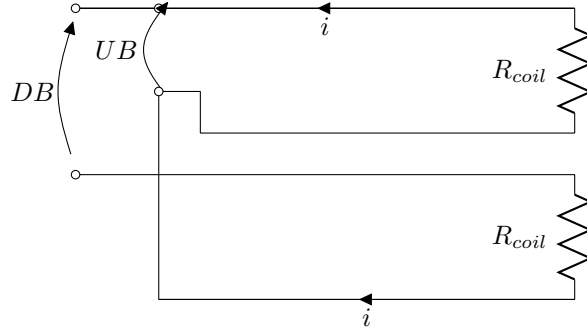


Figure 2: Dipole bucking scheme

2 Set-up and noise analysis

Measures were carried out inserting the probe in the magnet and connecting it to a stepper motor. The angular position is acquired using an angular encoder that generates TTL pulses on two channels: one provides a pulse after each full turn of the probe; the other, instead, 1024 pulses evenly distributed during each single turn. The output of each coil is connected through a coaxial cable to the DAQ.

2.1 DAQ

2.1.1 NI-4462

Voltages coming from the coils and the angular encoder are sampled by two National Instruments PXI-4462 Dynamic Signal Analyzers. These cards employ a $\Sigma\Delta$ ADC with the following characteristics:

- Maximum sampling frequency: $204.8kHz$
- Fully-differential inputs
- Resolution: $24bit$
- Minimum input range: $\pm 0.316V$
- Differential input resistance: $1M\Omega$
- Coupling set on DC

The highest coil output resistance is about $10k\Omega$. Given the quite high DAQ input resistance, the signal will be reduced only by 1%. Using data about resolution and input range, it is possible to compute the theoretically minimum acquirable voltage (LSB) and the quantization noise (σ).

$$LSB = \Delta = \frac{0.316V \times 2}{2^{24}} \approx 37.67nV \quad \sigma = \frac{\Delta}{\sqrt{12}} \approx 10.87nV \quad (11)$$

In fact, noise picked up by the DAQ itself is higher than the quantization noise. Figure 3 shows the power spectrum of the sampled data coming from one channel terminated using a 50Ω resistor. As the bandwidth of interest for the harmonic analysis extends from 1 Hz up to about 100 Hz, taking a margin of 1 decade and applying Nyquist theorem, a sampling frequency of 2 kHz has been chosen. From the power spectrum, it is possible to infer that the white component of the noise has a power spectral density $\sqrt{S_f} \approx 1 \frac{nV}{\sqrt{Hz}}$. Neglecting the $1/f$ component, this means a total in-band noise power of approximately $1 \frac{nV}{\sqrt{Hz}} \times \sqrt{1kHz} \approx 32nV$: much higher than the quantization noise.

A better insight on the limits of the DAQ is presented in Table 1. $1/f$ noise component brings the total noise power to a value approximately 10 times higher than the one computed considering only white noise. This means that a significant improvement of the SNR can be achieved implementing a modulation scheme. Furthermore, the non negligible offset (few μV as reported in the table) can be a

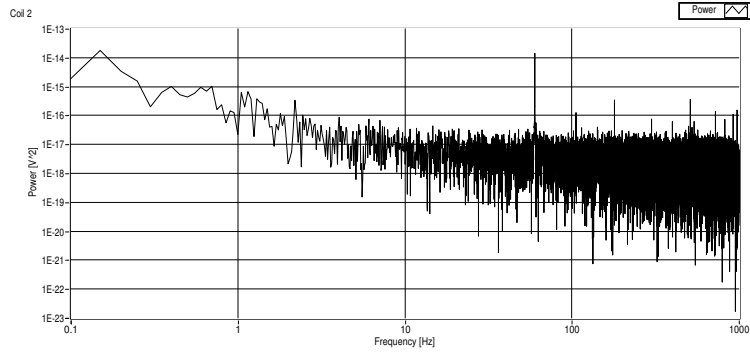


Figure 3: Noise Power Spectrum

Channel	Mean [μV]	Standard deviation [μV]
AI0	-12.04	0.46
AI1	5.34	0.36
AI2	0.53	0.44
AI3	4.64	7.08

Table 1: NI-4462 channels offset and noise

problem when computing the flux. A DC component suppression scheme has to be implemented in order to prevent drifts of the measured flux. Channel AI3 is affected by a particularly high noise. It follows that it should be used not to acquire signal coming from one of the coils, but to sample the ancillary signals like index pulses or encoder pulses.

2.2 Probes

Random magnetic field from the environment can significantly compromise harmonic measurements. Furthermore, as Morgan probes have an output resistance much lower than PCB probes, there could be differences in terms of noise and sensitivity between them. In the following paragraphs will be discussed if these differences are meaningful or not.

2.2.1 PCB probe

The PCB probe used provides five signals:

- Unbucked (UB)
- Dipole bucked (DB)
- Dipole quadrupole bucked (DQB)
- Dipole quadrupole sextupole bucked (DQSB)
- Unbucked low gain (UBL): same configuration as UB, but with less windings

How each signal impacts on the final result will be explained in section 4.

Figure 4 shows the power spectrum of the voltage induced in the unbucked coil when the probe is not spinning. The main harmonic added at 60 Hz is due to the fact that the probe acts like an antenna picking up signal coming from the AC power plug. It is interesting pointing out that the white noise level appears to be almost the same as the DAQ noise shown in figure 3. This can be explained as following. The main contribution to white noise comes from random motion of carriers in coil wires. The output resistance of the unbucked coil is about $1 \text{ k}\Omega$. Thus the white noise power density associated to it is $\sqrt{S_f} = \sqrt{4kTR_{coil}} \approx \sqrt{4kT \times 1 \text{ k}\Omega} \approx 4 \frac{nV}{\sqrt{\text{Hz}}}$: a value comparable to the DAQ white noise contribution. As noise contributions adds up quadratically, overall white noise is increased by a factor $\approx \sqrt{17}$ that is difficult to see in a logarithmic graph like the previous one.

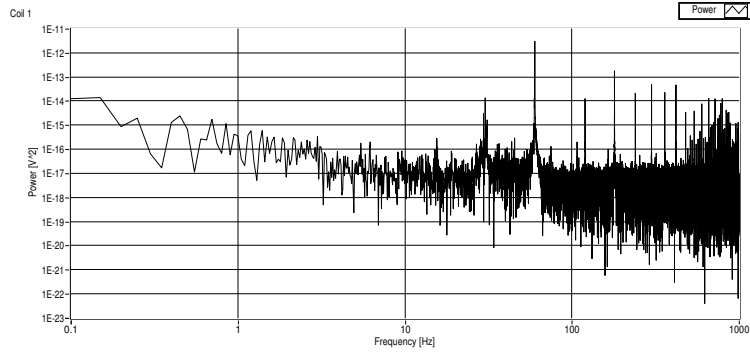


Figure 4: UB coil. Probe still

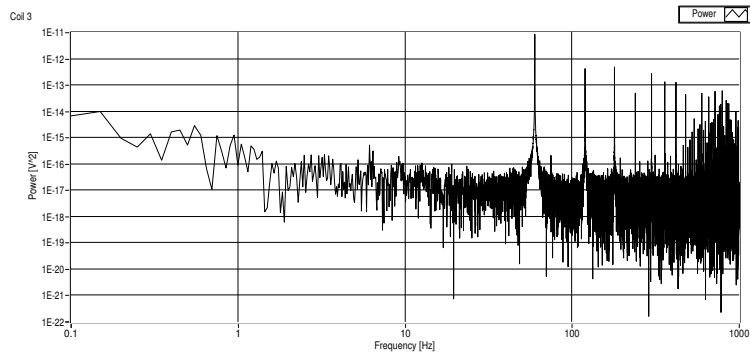


Figure 5: DQB coil. Probe still

Let's consider now the output of the dipole quadrupole bucked coil shown in figure 5. This winding has an higher output resistance than the unbucked one: approximately $4.5 \text{ k}\Omega$. Thus, its white noise power will be $\sqrt{S_f} = \sqrt{4kT \times 4.5 \text{ k}\Omega} \approx 8.5 \frac{\text{nV}}{\sqrt{\text{Hz}}}$. As this value dominates over DAQ noise, the overall white noise level is increased, as shown in figure 5. However, these variations are pretty small and it is not expected that they will affect the SNR when performing harmonic measures.

2.2.2 Morgan probe

As previously stated, Morgan probes use a different wiring layout. While bucking schemes try to suppress one or more harmonics, wires in this kind of probes are wound in such a fashion that each coil is sensitive (ideally) only to one harmonic. The probe used has 6 outputs: 2P1, 4P1, 6P1, 8P1, 10P1, 12P1; each one sensitive, respectively, to dipole, quadrupole, sextupole, octapole, decapole and dodecapole. As wires are machine-wound, they are thicker and the number of windings is fewer than in the PCB probe. Thus, the output resistance is much lower: just few Ω for all the windings. Basing on the considerations made in the previous section, it is possible to predict that the white noise measured is not due to the probe, but due to the DAQ.

This is confirmed by figures 6a and 6b: the white noise component has almost the same power in both cases and it is equal to the one measured when the DAQ inputs where terminated.

2.3 Stepper motor

As previously stated, when measuring harmonics the probe will be spun using a stepper motor. This kind of motors can introduce an important amount of white noise.

Figures 7a 7b show respectively the power spectrum of the PCB unbucked and Morgan dipole sensitive coils when the probe spins at 1 Hz. The peak at 2 Hz in 7a is due to residual magnetization of the quadrupole magnet and it is not present in 7b as the selected winding is not sensitive to quadrupole. As expected, white noise is much higher: from the previous $\sqrt{S_f} \approx 1 \frac{\text{nV}}{\sqrt{\text{Hz}}}$, it raised to $\sqrt{S_f} \approx 1 \frac{\mu\text{V}}{\sqrt{\text{Hz}}}$. The fact that it is the same in both probes proves that the noise source is not the probe, but the motor.

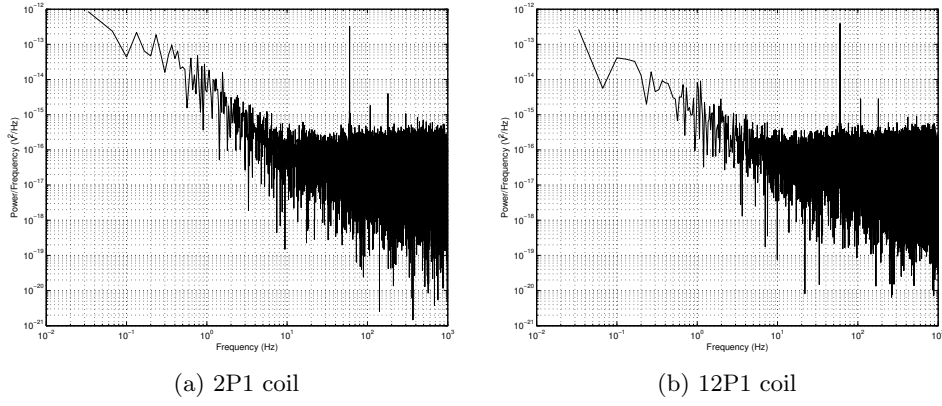


Figure 6: Morgan probe. Not spinning

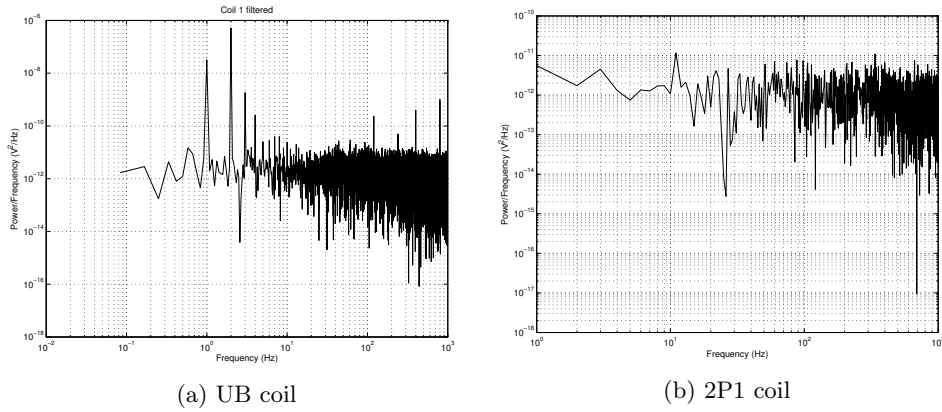


Figure 7: Probe spinning at 1 Hz

2.4 Power supply

Magnets were powered using a Kepco BOP 36-12M DC bipolar power supply. Random fluctuations of the current provided by it cause fluctuations of the flux through the coil and thus contribute to the overall noise power.

Figure 8 shows the power spectrum of the signal coming from the unbucked coil when the probe is inserted in the quadrupole magnet. Comparing it to figure 4, it is clear that the current generator has introduced a substantial amount of white noise. However, this amount is negligible with respect to the one introduced by the stepper motor.

2.5 Conclusion

The higher output resistance of PCB coils with respect to Morgan coils brings an increase of the white noise. However, this difference is negligible with respect to other noise sources. In particular, the stepper motor is what limits the sensitivity of the measurement system.

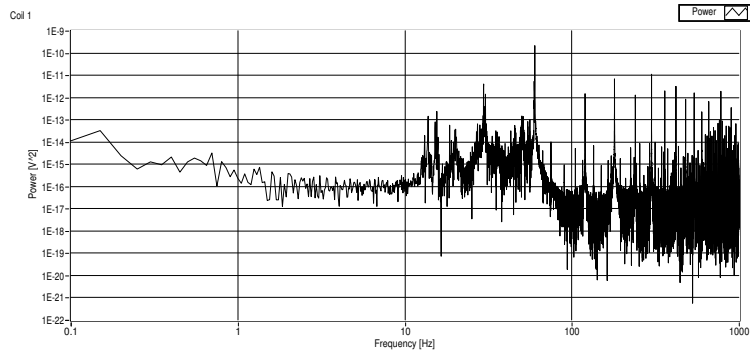


Figure 8: UB coil. Power supply on

3 LABView VI

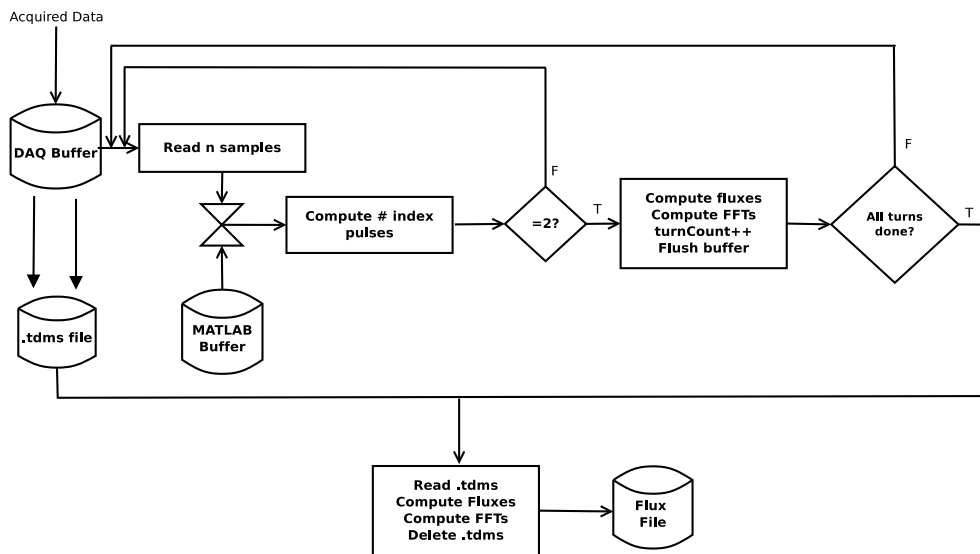


Figure 9: VI flowchart

Figure 9 shows the flowchart of the Virtual Instrument (VI) developed to measure the harmonics generated by the two magnets. The program let the user specify the number of turns to acquire, spinning frequency, sampling frequency and whether or not to save the results on a file. While voltages coming from coils and encoder are sampled, magnetic fluxes and their FFTs are computed and displayed. When all turns are acquired, the harmonic analysis is performed, showing a plot of the field and displaying both the normalized and not normalized harmonic components. Fluxes and harmonic coefficients computations are performed using a MATLAB script developed by Joe DiMarco, while the VI and field plotting have been developed by the supervisee. Samples coming from the ADC are continuously acquired, stored in the DAQ buffer and saved in a temporary *.tdms* file. An inner loop reads n samples from the DAQ buffer and keeps on storing them in a separate buffer until a full turn has been acquired. Then, the voltages are integrated in order to obtain the magnetic fluxes through each coil and their FFT is computed and plotted. This allows to show almost real-time the result of the measures. The process is repeated until all turns are acquired. Finally, all the buffers are flushed and the *.tdms* file containing the raw data is read and the harmonic analysis is performed. It has been chosen not to perform the harmonic analysis at each single step but just at the end of the whole acquisition to prevent buffer-overflow problems and artifacts in the Fourier analysis due to accidentally skipped samples.

4 Measures

Harmonics generated by a quadrupole and a dipole magnet were measured using both probes. The dipole was powered with 10 A, thus generating a magnetic field of $C_1 \approx 71$ mT at reference radius $R_{ref} = 10$ mm. On the other hand, the quadrupole was biased at 5 A. With this current, it generates $C_2 \approx 2$ mT at reference radius $R_{ref} = 10$ mm. To suppress stray fields, measures were taken with both positive and negative currents and results combined. Automatic coil coefficients calibration was performed in the case of PCB probe when measuring the quadrupole field with the PCB probe in order to take into account misalignments of the board. The results of this calibration were used when measuring the dipole, as automatic calibration is not possible when the second order harmonic is not dominant. Each set of measures is obtained computing mean and standard deviation of 10 consecutive measures.

4.1 Dipole magnet

Signal	f	2	3	4	5	6
Morgan	1 Hz	942.79	313.68	147.84	60.925	47.62
	2 Hz	302.1769	127.94	48.68	24.47	16.56
	4 Hz	118.72	56.38	20.29	10.01	5.80
UB	1 Hz	1639.4	722.62	343.60	169.56	97.81
	2 Hz	2192.6	941.77	461.47	242.49	130.27
	4 Hz	4347.6	1918.8	972.95	541.37	320.75
DB	1 Hz	91.46	36.64	12.31	7.06	4.32
	2 Hz	27.64	9.71	3.49	1.75	1.48
	4 Hz	24.50	8.20	4.72	2.57	1.52
DQB	1 Hz	91.46	70.71	17.06	9.62	5.36
	2 Hz	27.64	24.31	8.52	3.33	2.29
	4 Hz	24.50	40.10	16.49	7.97	4.77
DQSB	1 Hz	91.46	70.71	56.22	20.55	10.01
	2 Hz	27.64	24.31	35.22	11.70	6.05
	4 Hz	24.50	40.10	77.58	30.37	14.66
UBL	1 Hz	1840.0	775.48	354.72	165.92	90.27
	2 Hz	2234.9	922.66	446.30	237.70	123.91
	4 Hz	4312.0e	1885.3	944.94	518.58	302.56

Table 2: Standard deviation value σ_{C_n} in milliunits. Dipole magnet

Table 6 summarizes all the measures taken on the dipole magnet. Tables showing relative error defined as $\epsilon = \frac{\sigma_{C_n}}{|C_n|}$ and absolute mean value $|C_n|$ can be found in appendix A.

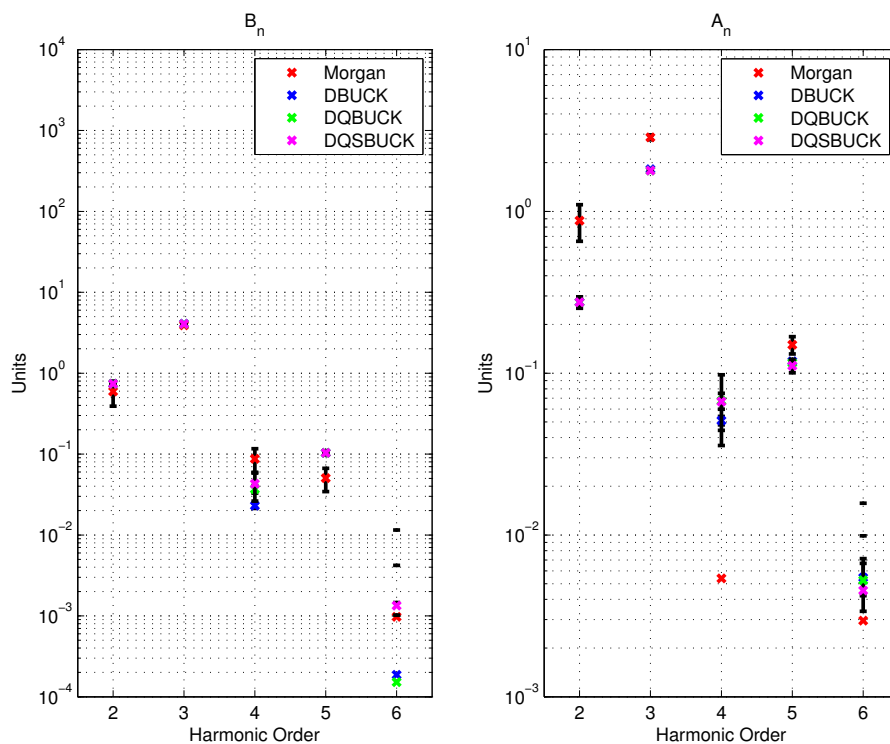
As stated at the beginning of this report, bucking is important to minimize the impact of probe vibrations on the harmonic measurement. This is clearly proven by table 6. As a matter of fact, signals coming from unbucked coils are much noisier than all the other cases. Furthermore, ϵ increases as the spinning frequency increase, supporting this hypothesis. It is also interesting pointing out UB and UBL coils generate a signal affected by almost the same level of uncertainty. This happens because, as shown in section 2.2, thermal noise have little effect on the overall noise. Thus, reducing the output resistance of the coil does not affect the overall noise that, in this case, is due to probe vibrations.

The PCB probe performs better than the Morgan one. The higher number of windings of the former probe, but the same noise level, increases the SNR .

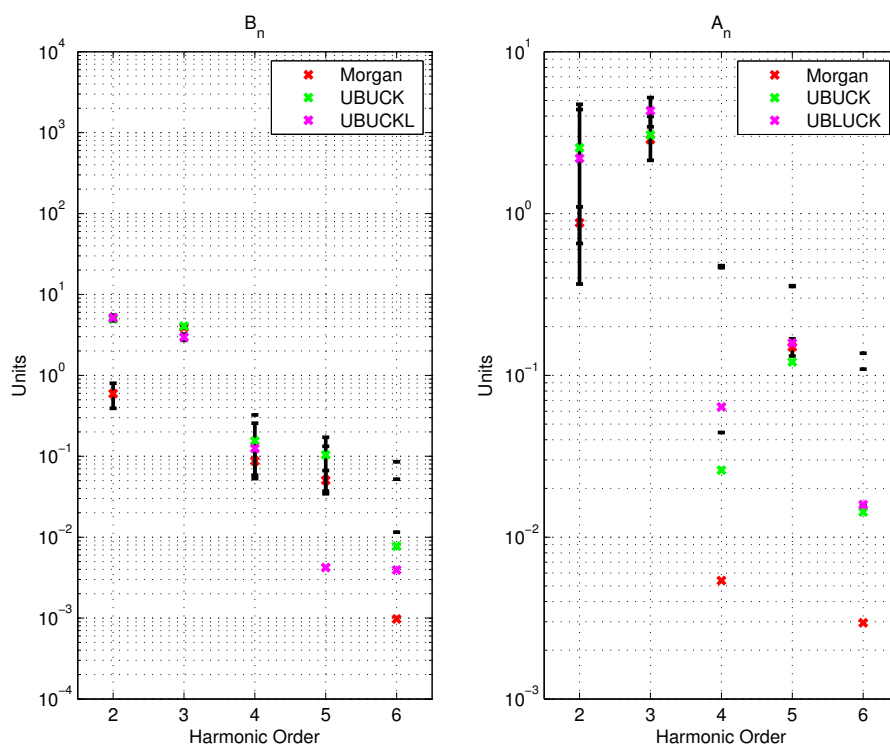
The relative error is a function of the spinning frequency. In the case of Morgan coils, ϵ decreases as the probe spins faster. The PCB probe, instead, performs better at 2 Hz. This happens because the latter probe has a not cylindrical symmetric geometry like the Morgan probe: vibrations increase a lot at 4 Hz and bucking is not enough to suppress spurious harmonics.

Figure 10a gives a better insight on the performances of the sensors employed. The unbucked signal has been omitted as it is too much affected by vibrations. Normal components measured by Morgan and PCB probes are in agreement, while skew components are slightly different. This can be due to a misalignment of the windings of the two probes and due to the fact that no centering correction was performed. The importance of bucking is furthermore stressed in figure 10b: both the unbucked and

unbucked low gain signals are not only affected by an higher uncertainty, but also they differ more from the mean value measured using the Morgan probe.



(a) Bucked



(b) Unbucked

Figure 10: Dipole harmonics comparison: normal component B_n and skew component A_n . Error as $\pm\sigma$

4.2 Quadrupole magnet

Performing the harmonic analysis, few problems linked to the signs of the calibration coefficients of the Morgan probe arose. As correcting them would require quite a lot of effort in terms of time, it has been chosen to perform the comparison not on normal and skew components of the magnetic field separately, but just on the magnitude.

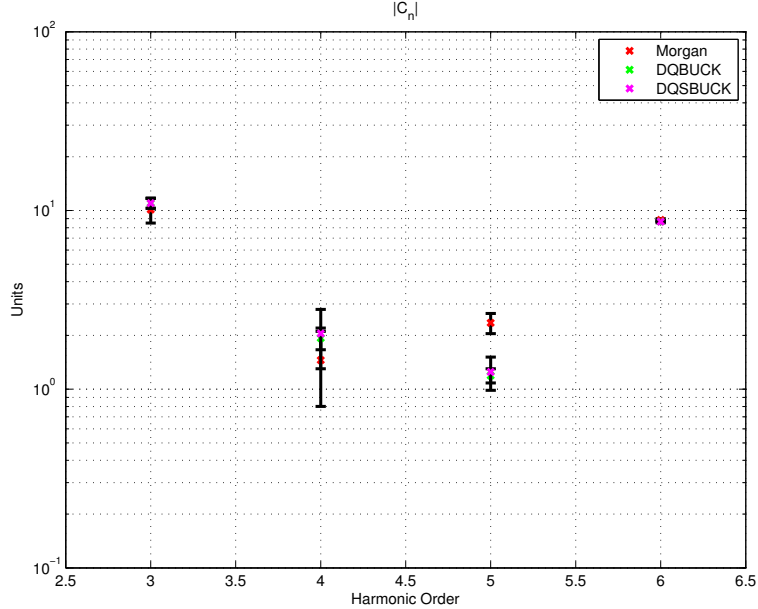


Figure 11: Bucked

Figure 11 shows the results obtained. Unbucked signals have been omitted as they are too much sensitive to vibrations as explained in the previous section. As happened for the dipole magnet, the two probes strongly agree on the value of the allowed harmonic ($n = 6$ for a quadrupole). Other values are still quite in agreement.

Signal	f	2	3	4	5	6
Morgan	1 Hz	26957	11313	6023.7	2831.9	996.26
	2 Hz	11694	3736.1	1479.0	810.32	412.03
	4 Hz	6151.8	1610.5	652.78	303.33	145.48
DQB	1 Hz	6382.5	1891.4	772.80	334.49	181.74
	2 Hz	3059.3	703.09	268.72	108.98	64.55
	4 Hz	7778.9	536.55	182.69	114.49	57.79
DQSB	1 Hz	6382.5	1891.4	1929.5	676.43	325.13
	2 Hz	3059.3	703.09	747.70	262.55	131.54
	4 Hz	7778.9	536.55	554.74	254.58	118.683

Table 3: Standard deviation value σ_{C_n} in milliunits. Quadrupole magnet

Table 3 further shows the better performances of the PCB probe.

5 Conclusions

Measures performed with PCB coils are in agreement with one performed using a more traditional technology like Morgan coils. The higher output resistance is not a problem in terms of thermal noise as it is comparable to the DAQ noise and the resolution of the acquisition system is limited by the stepper motor. Signal reduction due to not infinite input resistance of the acquisition system is tolerable when performing harmonic analysis. It is not negligible when measuring field strength. However, it can easily

compensated. Thanks to their higher gain and same noise, the simpler geometry and the more precise wire placement, PCB coils have a better resolution than Morgan coils. Their accuracy can be further improved replacing the stepper motor with a less noisy one and improving the geometry of the probe in order to reduce vibrations.

A Additional tables

Signal	f	2	3	4	5	6
Morgan	1 Hz	1.00	4.70	68.67×10^{-3}	162.14×10^{-3}	3.11×10^{-3}
	2 Hz	1.06	4.84	87.66×10^{-3}	158.21×10^{-3}	3.11×10^{-3}
	4 Hz	1.08	4.82	86.45×10^{-3}	157.86×10^{-3}	10.10×10^{-3}
UB	1 Hz	5.76	5.17	101.59×10^{-3}	179.20×10^{-3}	13.66×10^{-3}
	2 Hz	5.57	5.08	156.80×10^{-3}	159.67×10^{-3}	16.26×10^{-3}
	4 Hz	5.76	5.12	170.95×10^{-3}	168.69×10^{-3}	36.22×10^{-3}
DB	1 Hz	786.07×10^{-3}	4.48	59.10×10^{-3}	156.21×10^{-3}	4.71×10^{-3}
	2 Hz	788.83×10^{-3}	4.48	55.94×10^{-3}	157.13×10^{-3}	5.44×10^{-3}
	4 Hz	782.52×10^{-3}	4.49	55.67×10^{-3}	159.07×10^{-3}	5.43×10^{-3}
DQB	1 Hz	786.07×10^{-3}	4.45	80.52×10^{-3}	154.27×10^{-3}	4.55×10^{-3}
	2 Hz	788.83×10^{-3}	4.44	76.90×10^{-3}	155.23×10^{-3}	5.25×10^{-3}
	4 Hz	782.52×10^{-3}	4.44	78.30×10^{-3}	157.17×10^{-3}	5.29×10^{-3}
DQSB	1 Hz	786.07×10^{-3}	4.45	87.67×10^{-3}	145.53×10^{-3}	3.43×10^{-3}
	2 Hz	788.83×10^{-3}	4.44	79.32×10^{-3}	151.88×10^{-3}	4.74×10^{-3}
	4 Hz	782.52×10^{-3}	4.44	83.97×10^{-3}	155.01×10^{-3}	4.50×10^{-3}
UBL	1 Hz	5.86	5.32	105.84×10^{-3}	157.84×10^{-3}	17.33×10^{-3}
	2 Hz	5.60	5.24	140.25×10^{-3}	158.42×10^{-3}	16.38×10^{-3}
	4 Hz	5.76	5.26	150.69×10^{-3}	164.47×10^{-3}	34.65×10^{-3}

Table 4: Mean value $\overline{|C_n|}$ in units. Dipole magnet

Signal	f	2	3	4	5	6
Morgan	1 Hz	0.96	66.40×10^{-3}	2.1529	0.38	15.30
	2 Hz	0.28	26.44×10^{-3}	0.55	0.15	5.32
	4 Hz	0.11	11.71×10^{-3}	0.23	63.43×10^{-3}	0.57
UB	1 Hz	0.28	0.14	3.38	0.95	7.16
	2 Hz	0.39	0.18	2.94	1.52	8.01
	4 Hz	0.75	0.37	5.69	3.21	8.85
DB	1 Hz	0.12	8.1724×10^{-3}	0.21	45.17×10^{-3}	0.92
	2 Hz	35.04×10^{-3}	2.17×10^{-3}	62.37×10^{-3}	11.16×10^{-3}	0.27
	4 Hz	31.315×10^{-3}	1.83×10^{-3}	84.86×10^{-3}	16.15×10^{-3}	0.28
DQB	1 Hz	0.12	15.89×10^{-3}	0.21	62.40×10^{-3}	1.18
	2 Hz	35.04×10^{-3}	5.47×10^{-3}	0.11	21.441×10^{-3}	0.43
	4 Hz	31.315×10^{-3}	9.04×10^{-3}	0.21	50.70×10^{-3}	0.90
DQSB	1 Hz	0.12	15.89×10^{-3}	0.64	0.14	2.92
	2 Hz	35.04×10^{-3}	5.47×10^{-3}	0.44	77.05×10^{-3}	1.28
	4 Hz	31.315×10^{-3}	9.04×10^{-3}	0.92	0.19	3.26
UBL	1 Hz	0.31	0.15	3.35	1.05	5.21
	2 Hz	0.40	0.17	3.18	1.50	7.56
	4 Hz	0.75	0.36	6.27	3.15	8.73

Table 5: Relative error ϵ . Dipole magnet

Signal	f	2	3	4	5	6
Morgan	1 Hz	2.69	1320.2	3456.3	1116.7	112.35
	2 Hz	1.17	333.95	845.70	305.09	47.10
	4 Hz	0.61	160	450	130	16.43
DQB	1 Hz	0.64	181.23	752.33	293.31	20.94
	2 Hz	0.30	63.91	139.16	91.42	7.44
	4 Hz	0.78	49.47	100	91.36	6.70
DQSB	1 Hz	0.64	181.53	2755.2	613.97	37.49
	2 Hz	0.30	64.00	364.94	210.23	15.19
	4 Hz	0.78	49.52	0.33	190	13.85

Table 6: Relative error $\epsilon \times 10^{-3}$. Quadrupole

References

- [1] M. Buzio. Fabrication and calibration of search coils. CERN-2010-004, pp. 387-421, 2011.
- [2] J. DiMarco et al. Application of PCB and FDM Technologies to Magnetic Measurement Probe System Development. 2012.
- [3] J. DiMarco, D.J. Harding, V. Kashikhin, S. Kotelnikov, M. Lamm, A Makulski, R. Nehring, D. Orris, P. Schlabach, W. Schappert, C. Sylvester, M. Tartaglia, J. Tompkins, and G. V. Velez. A fast-sampling, fixed coil array for measuring the ac field of fermilab booster corrector magnets. *Applied Superconductivity, IEEE Transactions on*, 18(2):1633–1636, June 2008.
- [4] L. Walckiers. Magnetic measurement with coils and wires. CERN-2010-004, pp. 357-385, 2011.
- [5] Andrzej Wolski. Maxwell’s equations for magnets, 2011.